Published in: Chemical Physics (2001), vol. 272, pp. 259-275.
Status: Postprint (Author's version)

The vacuum UV photoabsorption spectrum of methyl chloride (CH_3Cl) and its perdeuterated isotopomer CD_3Cl
I. A Rydberg series analysis

R. Locht [a], B. Leyh [a,1], A. Hoxha [a], H.W. Jochims [b], H. Baumgärtel[b]

[a] *Département de Chimie Générale et de Chimie Physique, Institut de Chimie, Bât.B6c, Université de Liège, Sart-Tilman par B-4000 Liège 1, Belgium*
[b] *Institut für Physikalische und Theoretische Chemie, Freie Universität Berlin, Takustraße 3, D-14195 Berlin, Germany*

Abstract

The vacuum UV photoabsorption spectrum of CH_3Cl has been recorded between 6 and 25 eV. A large number of vibronic bands are observed. These were partly ascribed to vibrationless Rydberg transitions. In the high photon energy range of 12-25 eV, very weak diffuse bands are mostly assigned to transitions from the $3a_1$, 1e and $2a_1$ to 3s orbitals. In the 6-12 eV photon energy range, numerous weak to strong bands are observed. The sharpness is very variable over the entire spectral region. In a first step, the interpretation of the spectrum and the assignment of the Rydberg transitions is based on the simple Rydberg formula. The observed features are classified in two groups of four series, each converging to one of the two spin-orbit components of the $\tilde{X}^2E$ state of CH_3Cl^+. Rydberg series of $n$sa$_1$ (δ = 1.069 and 1.064), $n$pa$_1$ (δ = 0.68 and 0.66), $n$pe (δ = 0.438 and 0.427) and nd (δ = -0.040 and -0.092) characters are observed. The same measurements have been made for the first time on CD_3C1 in the 6-12 eV photon energy range. The same Rydberg transitions are observed. Analogous series are characterized by about the same δ values: $n$sa$_1$ (δ = 1.038 and 0.968), $n$pa$_1$ (δ = 0.65 and 0.61), $n$pe (δ = 0.458 and 0.462) and nd (δ = -0.004 and -0.082). Ionization energies for CD_3Cl $\tilde{X}^2E_{3/2}$ at 11.320 eV and $\tilde{X}^2E_{1/2}$ at 11.346 eV are deduced. In a second step, we fitted the experimental data for the $n$sa$_1$ and $n$pa$_1$ states to an energy expression taking into account both the exchange interaction and the spin-orbit coupling. This accounts for the progressive switching from Hund's case (a) to Hund's case (c).

1. Introduction

The still acute problem of the detrimental effects of the atmospheric pollutants is a main reason for the interest arisen for the organic halogenated compounds and more particularly the various halogenated methanes. The most abundant of these species in the upper atmosphere is mono-chloromethane (CH_3Cl), mainly produced by biological processes such as wood combustion, biomass burning and oceanic emission [1]. Other monohalomethanes and mixed halomethanes (freons) are released in the atmosphere essentially by man-made sources. They have been recognized as having profound effects on the atmospheric ozone layer [2]. This fact became a strong incentive for numerous investigations on these compounds.

Another motivation to investigate these compounds is related to our ongoing study of the excitation, ionization and monomolecular dissociation dynamics of their molecular ions. We extensively examined the vacuum UV spectroscopy, the photoelectron spectroscopy (TPES and He-I) and the mass spectrometric photoionization of the halogenated derivatives of methane and ethylene. For many cases, the major importance of the localization and identification of neutral molecular states embedded in the ionization continua has been demonstrated [3-7].

The halogen substituted derivatives of methane have been thoroughly studied in the last fifteen years [8,9] using most of the available spectro-scopic techniques. The monosubstituted species received much less attention, excepting mono-chloromethane CH_3Cl. Its photoabsorption spectrum has been reported several times, in different wavelength regions and under different experimental conditions. To the best of our knowledge, the photoabsorption spectroscopy of the perdeuterated isotopomer CD_3Cl has been reported only once in the 165-145 nm wavelength region [10].

The first observation of the vacuum UV photoabsorption spectrum of CH_3Cl was reported by Price [11] in the wavelength region of 100-200 nm (6.2-12.4 eV) using a grazing incidence monochromator and the Lyman continuum as excitation source. The observed bands were classified into two Rydberg series converging to the two first ionization limits, assigned to two components separated by 650 cm^{-1}. Relatively weak absorptions were attributed to vibrational bands.

[1] Chercheur Qualifié FNRS (Belgium).

Russell et al. [12] and Raymonda et al. [13] systematically investigated the chloromethanes and the alkyl chlorides in the 50 000-90 000 cm^{-1} (6.20-11.16 eV) region. The extinction coefficients were measured and Rydberg transitions were assigned for methyl chloride. The splitting of about 880 cm^{-1} [12] or 900 cm^{-1} [13] measured between two peaks observed at 62 580 and 63 460 cm^{-1} [12] or at 62 570-63 470 cm^{-1} was ascribed to the spin-orbit coupling and a few vibrational modes were identified in the first Rydberg transition. Hoch-mann et al. [14] and Felps et al. [10] studied the Rydberg transitions in the methyl halides. As mentioned earlier, the latter group [10] also examined the lowest Rydberg transitions in the perdeuterated methyl halides.

The most extensive study of the vacuum UV photoabsorption spectrum of CH_3Cl has been reported by Truch et al. [15]. The spectrum was investigated in the wavelength region of 68 600-94 700 cm^{-1} (8.50-11.74 eV). Valence-shell and Rydberg transitions were observed and assigned. The vibrational fine structure in this energy range was analyzed in some detail for the first time.

Using synchrotron radiation Wu et al. [16] were able to extend the observation of the photoabsorption spectrum of various fluoro- and chloromethanes well beyond the 11.8 eV (95 000 cm^{-1}) limit. These authors found members of Rydberg series converging to higher lying ionization energies. Discrete structure in the 57.8-62.0 nm (20.00-21.45 eV) region was ascribed to the vibrational structure of a Rydberg state, member of a series converging to the $4a^{-1}$ ionization limit at 21.5 eV. Using the same light source Lee and Suto [17] investigated the fluorescence and the photoabsorption spectra of the chloromethanes. No analysis of the latter spectrum has been reported in this work.

Though usually less resolving in this energy range, the electron energy loss spectroscopy provides very useful information on molecular structure. Fairly recently, high resolution (0.05 eV FWHM) dipole (e,e) measurements were reported by Olney et al. [18] between 6 and 25 eV. They also measured the absolute oscillator strength (related to the cross section and to the extinction coefficient) for photoabsorption of CH_3Cl between 6 and 350 eV at low resolution (1 eV FWHM).

In the present contribution made of two sequential papers, we report on the photoabsorption spectrum of CH_3Cl measured in the 6-25 eV photon energy range using synchrotron radiation. To the best of our knowledge, the photoabsorption spectrum of CD_3Cl, as observed between 6 and 12 eV photon energy will be reported for the first time. The aim of this paper is to reinvestigate in detail the vibrationless Rydberg transitions in CH_3Cl and CD_3Cl.

2. Experimental

2.1. Experimental setup

The experimental setup used in this work has already been described in detail elsewhere [19]. Only the most salient features will be reported here.

Synchrotron radiation available from the BESSY I facility (Berlin, Germany) is dispersed with a modified vacuum UV normal incidence 225 McPherson monochromator with a focal length of 1.5 m, instead of 1 m in the commercial version (1m-NIM-2 beamline). A laminar Zeiss grating is used for the efficient reduction of the 2nd spectral order. It is gold coated with 1200 l/mm and its transmission breaks down above 26 eV (210000 cm^{-1} or 47 nm). The width of the entrance and exit slits of 100 μm provides a 0.1 nm resolution. The light passes through a 1 mm thick stainless steel microchannel plate necessary to ensure a differential pressure of 1:1000 before entering a 30 cm long stainless steel absorption cell. Most of the spectra are recorded without filter on the light path. However, in some cases a LiF filter is used, which can be inserted in the light beam without vacuum breakdown. This filter has a transmission cutoff at 11.8 eV (95 000 cm^{-1} or 105 nm). The vapor pressure in the cell is measured by a Balzers capacitor manometer. The light is detected by a sodium salicylate sensitized photomultiplier located at the end of the absorption cell and in front of the absorption cell entrance slit. Output pulses are recorded by a 100 MHz counter. The recording of an absorption spectrum requires one scan with gas in the absorption cell and one with the empty cell. The stability of the synchrotron radiation and of the pressure in the cell allowed us to ensure reliable absorption data. If required, the spectra presented in the following sections are corrected for any pressure drift. The commercially available CH_3Cl, purchased from Praxair and of 99.5% purity, was used without further purification. The CD_3Cl, purchased from Merck, Sharp and Dohme, is certified at 99 at.% purity. No noticeable impurity was observed by mass spectrometry at 21.2 eV photon energy. Therefore, the sample was used without further purification.

2.2. Data handling and error estimation

As will be mentioned in the next section, in the high photon energy part of the absorption spectrum weak and diffuse structures are superimposed on a strong continuum. To facilitate the characterization of these features, a continuum subtraction procedure has been applied. This has already been used successfully in previous spectral analysis [20,21]. For this purpose, the experimental curve is severely smoothed to simulate the underlying

continuum which is then subtracted from the original photoabsorption spectrum. The smoothing procedure consists in filtering the experimental curve by fast Fourier transform. The weak features emerge from a remaining very weak background.

The wavelength calibration of the monochromator has been performed by using the Ar^+ absorption spectrum between the $^2P_{3/2}$ and the $^2P_{1/2}$ ionic states. The accuracy of this calibration was better than 2 meV. In the measurements extending from 6 to 25 eV photon energy, the photoabsorption spectrum has been recorded with an energy interval of about 10 meV. The error on the energy position of a feature is estimated to be 15 meV. In the photoabsorption spectra extending between 6 and 12 eV photon energy, an energy increment of 1.5 meV has been adopted. The error on the energy position of a feature is estimated to be of the order of 2 meV. This evaluation is confirmed by the reproducibility of energy positions measured in four different spectra recorded in a two years interval.

3. Experimental results

3.1. The CH_3Cl photoabsorption spectrum

The photoabsorption spectrum of CH_3Cl has been measured between 6 and 25 eV photon energy. A typical coarse recording (with energy interval of 10 meV) is reproduced in Fig. la where the molar extinction coefficient $\varepsilon_{h\nu}$ is plotted as a function of the photon energy. Particular attention has been brought to the energy range of 11-25 eV where the subtraction procedure (see Section 2.2) has been applied to enhance the weak and broad bands. The result is shown in Fig. lb. Due to the scattering of the "difference" signal Δ, a FFT- smoothed curve has been drawn through the data points. The energy positions of these weak bands are listed in Table 1 together with the assignments proposed in this work.

Table 1 *Position in energy (eV) of Rydberg transitions, as defined by their band maxima, observed between 11 and 25 eV photon energy*

Band maxima			Conv. limit [22,23]	Assignment, n^*—Rydb. trans.
This work	[18]	[16]		
	11.64	11.6	14.4—$3a_1^{-1}$	2.022 $3a_1 \rightarrow 3s$
12.10	-		16.0—$1e^{-1}$	2.024 $1e \rightarrow 3s$
13.10	13.6		16.0—$1e^{-1}$	2.422 $1e \rightarrow 3p$
14.10	14.5		16.0—$1e^{-1}$	3.246 $1e \rightarrow 4s$
16.2-16.8	16.7 (max)		20.1—?[a]	2.000 $?\rightarrow 3s$[a]
19.07	19.0		21.6—$2a_1^{-1}$(?)	2.333 $2a_1(?) \rightarrow 3s$
-	20.0	20.29-21.16	21.6—$2a_1^{-1}$(?)	- [$2a_1 \rightarrow 4d$][b]

Convergence limits data refer to the vertical ionization energy (IE_v) values.
[a] For explanation, see text.
[b] Data in brackets from Ref. [16].

Energy positions estimated from the dipole (e,e) cross-section curve as reported by Olney et al. [18] and from the high energy photoabsorption curve published by Wu et al. [16] are inserted in this table. The convergence limits listed in this table are those reported by Karlsson et al. [22] and by Von Niessen et al. [23] and obtained by the He(I) and He(II) resonance lines respectively. Question marks indicate uncertainty on the assignments of convergence limits [24].

The fine structured energy region has been recorded between 6 and 12 eV (with energy increments of 1.5 meV). An overview of the spectrum is shown in Fig. 2a where the molar extinction coefficient is plotted as a function of the photon energy. In the same figure the assignment of the main features to series of vibrationless Rydberg transitions has been inserted. The convergence limits are the ionization energy values reported by Karlsson et al. [22] as measured by He(I) photoelectron spectroscopy. Fig. 2b shows the photoabsorption spectrum close to the ionization limit on an expanded photon energy scale. The assignments are inserted in the figure by vertical bars.

Published in: Chemical Physics (2001), vol. 272, pp. 259-275.
Status: Postprint (Author's version)

Fig. 1. *(a) The vacuum UV photoabsorption spectrum of CH_3Cl in the 6-25 eV photon energy range. The successive ionization continua are indicated, (b) The intensity difference Δ between the photoabsorption spectrum (PAS) and the strongly smoothed photoabsorption spectrum (SSPA) plotted as a function of the photon energy in the 12-24 eV range. The continuous curve is the result of a FFT smoothing. The assignments of the structures are indicated by vertical bars.*

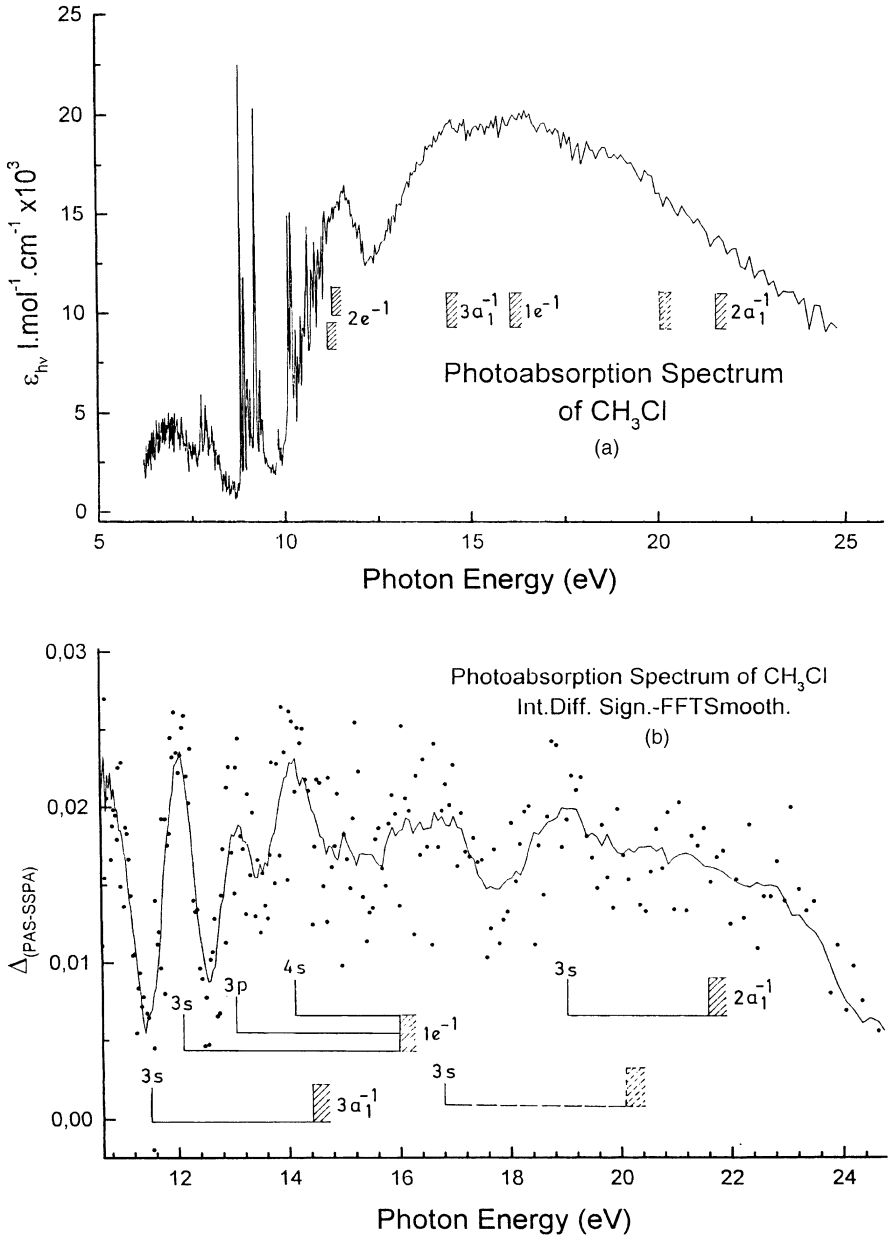

3.2. The CD_3Cl photoabsorption spectrum

The photoabsorption spectrum of CD_3Cl has been recorded between 6 and 12 eV photon energy. In Fig. 3a the molar extinction coefficient ε_{hv} is plotted as a function of the photon energy. The series of vibrationless Rydberg transitions, as assigned in this work are inserted in this figure together with their convergence limit as taken from an ongoing photoelectron spectroscopic work [25].

The high energy features, i.e. about 0.5 eV below the ionization limits, and their assignments are shown on an expanded photon energy scale in Fig. 3b, together with the ionization energies of CD_3Cl in both spin-orbit components.

Published in: Chemical Physics (2001), vol. 272, pp. 259-275.
Status: Postprint (Author's version)

Fig. 2. *(a) The vacuum UV photoabsorption spectrum of CH_3Cl in the 6-12 eV photon energy range. Vibrationless Rydberg transitions and their respective convergence limits are indicated by vertical bars. (b) Detail of the photoabsorption spectrum of CH_3Cl close to the first ionization limit. The assignments are indicated by vertical bars.*

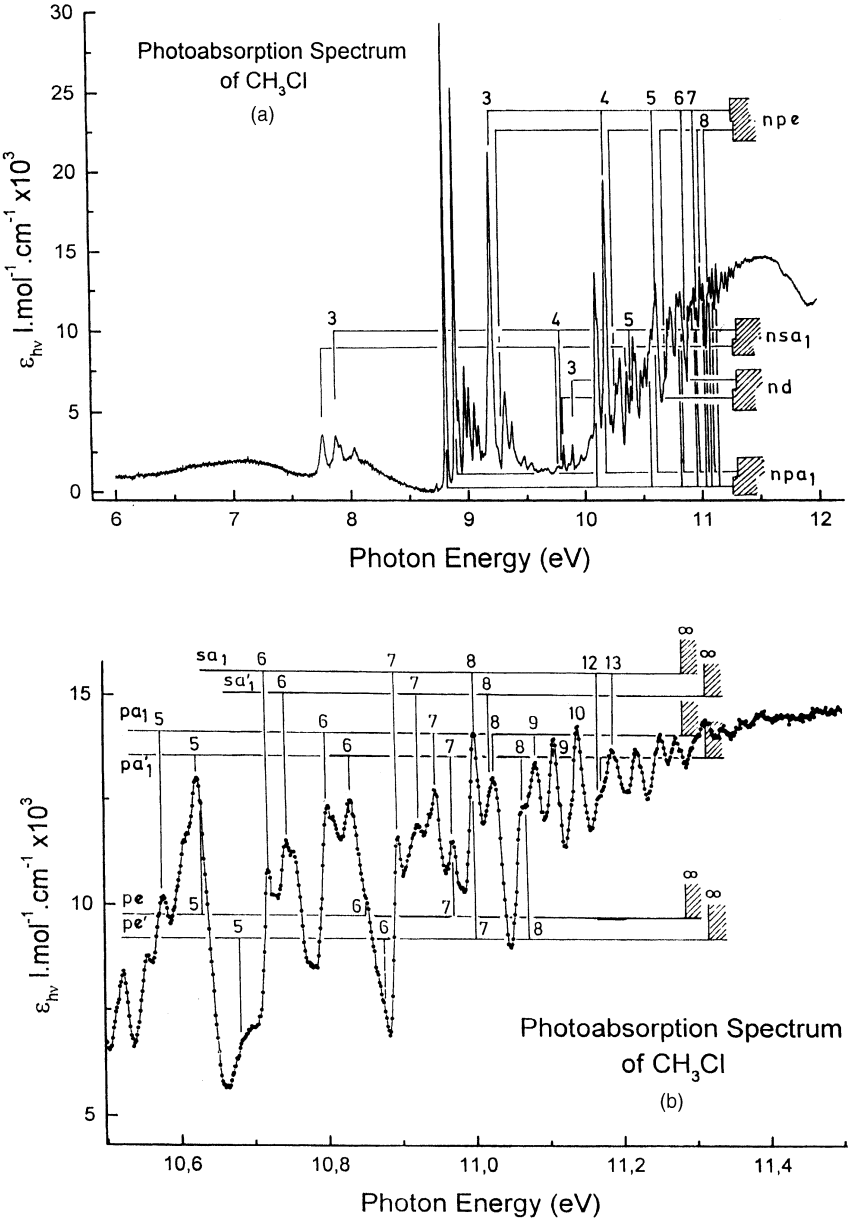

4. Discussion of the experimental data

For clarity in the following discussion of the experimental results, the molecular orbital configuration of CH_3Cl in the C_{3v} point group is reminded, i.e.

$$Cl(1s^2)C(1s^2)Cl(2s^22p^6)(1a_1)^2(2a_1)^2(1e)^4(3a_1)^2(2e)^4: \tilde{X}^1A_1$$

where the first atomic-like orbitals correspond to the inner-shell orbitals which are localized on the Cl and C atoms and have 1s, 2s and 2p character. The $1a_1$ and $2a_1$ correspond to the inner-valence molecular orbitals whereas the le, $3a_1$ and 2e molecular orbitals have outer-valence character. The most accurate and well-resolved He(I) photoelectron spectrum [22] provides the adiabatic ionization energies at 11.289 ± 0.003 eV ($2e^{-1}$), 13.8 eV ($3a_1^{-1}$) and at 15.4 eV ($1e^{-1}$) successively. The lowest ionic state shows a $^2E_{3/2}$-$^2E_{1/2}$ spin-orbit splitting of 27 ± 6 meV (218 ± 48 cm^{-1}) [22], with adiabatic ionization energies of 11.289 ± 0.003 and 11.316 ± 0.003 eV respectively. As will

be discussed in the accompanying paper, the strength of the Jahn-Teller distortion is small compared to the spin-orbit coupling. This situation is completely different from the CH_3F case [21].

Higher lying vertical ionization energies are located at 14.4 eV ($3a_1^{-1}$) and 16.0 eV ($1e^{-1}$) [22]. With the He(II) resonance line at 30.4 nm, the ionization of the inner-valence orbitals is possible and vertical ionization energies are measured at 21.2 eV ($2a_1^{-1}$) and at 24.1 eV ($1a_1^{-1}$) [18,23].

Fig. 3. *(a) The vacuum UV photoabsorption spectrum of CD_3Cl in the 6-12 eV photon energy range. Vibrationless Rydberg transitions and their respective convergence limits are indicated by vertical bars. (b) Detail of the photoabsorption spectrum of CD_3Cl close to the first ionization limit. The assignments are indicated by vertical bars.*

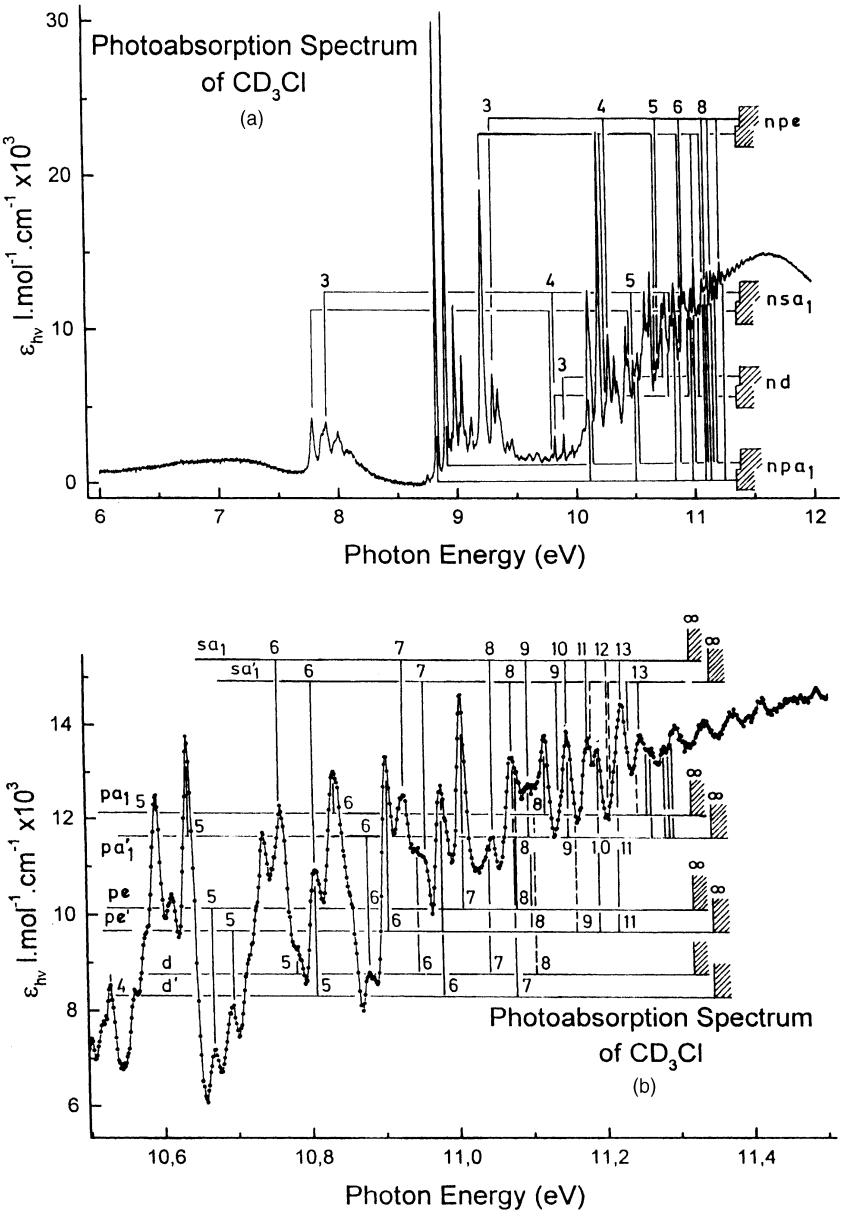

4.1. Remark about the absorption intensities

When comparing the shape of the photoabsorption curve represented in Fig. 1 with the high resolution dipole (e,e) curve reported by Olney et al. [18] (see Fig. 3 in Ref. [18]) a fairly large discrepancy is observed for the

intensity of the bands. Particularly the intensity of the quasi-con-tinuum above 12 eV photon energy is about twice as intense as in the photoabsorption spectrum. The intensities (all given by the molar extinction coefficient expressed in 10^3 $1mol^{-1}$ cm^{-1} units), as measured in the present work and estimated from earlier photoabsorption spectra [12,13,15-18] and dipole (e,e) measurements, are compared in Table 2 where absolute cross-sections ($\sigma_{h\nu}$ in Mb units) are converted to molar extinction coefficient ($\varepsilon_{h\nu}$) by using the expression [26]

$$\varepsilon_{h\nu}(1mol^{-1}\ cm^{-1}) = \sigma_{h\nu}\ (Mb) \times 6.0203 \times 10^2.$$

Except for the spectrum reported by Lee and Suto [17], the photoabsorption works are quite consistent with each other up to 10.2 eV. Discrepancies appear near the maximum at about 11.0-11.6 eV. However, at this energy the dipole (e,e) measurements exhibit a much larger value. This discrepancy is even larger at about 16 eV photon energy. Olney et al. [18] invoked 'line-saturation' errors arising from the logarithmic form of the Beer-Lambert law. The photoabsorption work of Lee and Suto [17] (see Table 2) would probably not fit in this explanation, the only agreement being observed for the intensity at 11.6 eV.

Table 2 *Comparison of molar extinction coefficient values ($\varepsilon_{h\nu}$ in 10^3 $1mol^{-1}$ cm^{-1} units) at different photon energies (eV) as measured by different authors by photoabsorption (Ph.Abs.) and dipole (e,e) spectroscopy*

hν (eV)	[12] Ph.Abs.	[13] Ph.Abs.	[15] Ph.Abs.	[16] Ph.Abs.	[17] Ph.Abs.	This work	[18] (e,e)
8.815	23.1	37.2	28.5	-	64.4	29.3	23.6
9.208	17.5	30.0	21.1	-	49.3	20.3	28.2
10.189	16.9	24.5	24.2	-	46.6	19.6	28.6
11.575	~14	13.9	17.5	-	36.2	14.8	35.1
~16	-	-	-	~39	-	20.3	48.1

For the cross-section to molar extinction conversion, see text.

4.2. The Rydberg series analysis

As clearly appears from the photoabsorption spectrum of CH_3Cl reproduced in Fig. 1, two distinct parts show up: (i) the low energy part extending from 6 to 11 eV and with an abundant fine structure and (ii) the high energy part spread over the 12-25 eV photon energy range, made of weak and broad bands. For the assignment of the features observed in this spectrum, their energy positions E_{Ryd} were first fitted to the Rydberg formula

$$E_{\mathrm{Ryd}} = \mathrm{IE} - \frac{R}{(n-\delta)^2} = \mathrm{IE} - \frac{R}{n^{*2}} \qquad (1)$$

where the Rydberg constant R = 13.6058 eV, δ is the quantum defect, n^* is the effective principal quantum number and IE is the convergence limit of the Rydberg series.

A more appropriate formula taking into account both exchange (singlet-triplet splitting) and spin-orbit coupling will be used in a second step of our analysis.

4.2.1. The high energy region

Concerning the high energy part, the available previous data are listed in Table 1 together with the data obtained in the present work. However, no assignments have been proposed in the literature, except for the 20.0 eV band [16] not observed in the present spectrum. The signal/noise ratio very likely prevents to detect this transition. Tentative assignments are proposed in the fifth column of Table 1 together with associated effective principal quantum numbers. The nature of these Rydberg states and their fate with respect to the unimolecular decomposition of the CH_3Cl^+ molecular ion will be discussed in a forthcoming paper [24].

The broad band observed in the 16.2-16.8 eV region behaves as a 3s Rydberg state, characterized by n^* = 2.00 if we assume a convergence limit of 20.1 eV. No such ionic state of CH_3Cl^+ has been mentioned in the literature. We recently investigated the threshold photoelectron spectrum of this molecule between 10 and 25 eV photon energy by using synchrotron radiation as a tunable excitation source [25]. A weak threshold photoelectron band spreads over the 19-21 eV energy range, has its maximum at 20.08 eV and has an intensity of about 30% of the 21.6 eV ionizing transition [24]. The presence of this weak signal is due either to (i) a direct ionizing transition or (ii) to the autoionization of a Rydberg state to a nearly resonant ionic state. This state could correspond to a doubly excited configuration. The Rydberg state at 16.2-16.8 eV could also be able to play a role in resonant dissociative ionization as it is the case for the CH_3^+ ion production from CH_3F [7] and for the $C_2H_3^+$ fragment from C_2H_3Br [4].

Published in: Chemical Physics (2001), vol. 272, pp. 259-275.
Status: Postprint (Author's version)

Table 3 *Vibrationless Rydberg transitions as observed for CH_3Cl in the present work and in previous reports [14] and [15] for both spin-orbit components: parts (a) and (b) converge to the 3/2 and 1/2 components of the ionic ^2E state respectively*

1. 2e → *n*sa$_1$					
This work				Literature data	
E_{Ryd} (eV)	E_{Ryd} (cm^{-1})	*n**	E_{Fit} (eV)	[15]	[14]
Part (a)					
7.759	62 582	1.963	7.759	-	62 578
9.742	78 576	2.965	9.745	[79 170][a]	79 271
10.422	84061	3.961	10.427	84095	83 623
10.722	86481	4.898	10.739	86 505	-
10.898	87 900	5.899	10.902	87 905	87 413
[11.004][a]	88 756	6.909	11.009	88 780	-
-	-	-		-	-
-	-	-		-	-
-	-	-		-	-
[11.175][a]	90134	10.925	11.176	90205	-
[11.193][a]	90280	11.905	11.194	-	-
Part (b)					
7.873	63 517	1.988	7.873	-	63 532
9.789	78 955	2.985	9.787	[79 800][a]	79 872
10.441	84214	3.943	10.457	84275	84 317
10.746	86 674	4.886	10.767	86775	86 655
10.927	88110	5.914	10.935	88215	88 028
[11.030][a]	88 965	6.897	11.036	89 000	-

2. 2e → *n*pa$_1$					
This work				Literature data	
E_{Ryd} (eV)	E_{Ryd} (cm^{-1})	*n**	E_{Fit} (eV)	[15]	[14]
Part (a)					
8.815	71 099	2.345	8.824	71 070	71 159
10.102	81 450	3.386	10.081	81 495	81 500
10.578	85 319	4.375	10.573	85 140	84 962
10.803	87 134	5.291	10.816	87 175	-
10.950	88 320	6.335	10.953	88 370	-
[11.030][a]	88 965	7.248	11.038	89 000	-
11.088	89 433	8.227	11.095	89 433	-
11.146	89 900	9.339	11.134	89 960	-
Part (b)					
8.895	71 744	2.371	8.919	71 735	71 823
10.193	82 190	3.476	10.122	82 275	82 041
10.624	85 690	4.434	10.604	85 780	-
10.834	87 384	5.313	10.844	87 365	87 413
10.974	88 497	6.280	10.981	88 525	-
11.068	89 271	7.407	11.065	89 271	-
11.113	89 634	8.188	11.122	89 660	-
[11.175][a]	90 134	9.423	11.161	90 205	-
[11.193][a]	90 280	10.517	11.189	90 365	-
-	-	-		90 440	-
11.226	90 546	12.295	11.227	-	-

3. 2e → *n*pe					
This work				Literature data	
E_{Ryd} (eV)	E_{Ryd} (cm^{-1})	*n**	*n*	[15]	[14]
Part (a)					
9.208	74 269	2.557	3	74 250	74 310
10.198	82 254	3.531	4	81 495	82 291

10.638	85 803	4.571	5	-	-
10.855	87 553	5.599	6	-	-
[10.972][a]	88 497	6.551	7	-	-
		Part (b)			
9.298	74 995	2.597	3	75 040	-
10.255	82 714	3.581	4	81 645	81 666
10.684	86 174	4.640	5	-	-
-	-	-	6	-	-
[11.004][a]	88 755	6.593	7	-	-
11.071	89 296	7.452	8	-	-

4. 2e → *n*d

This work				Literature data	
E_{Ryd} (eV)	E_{Ryd} (cm^{-1})	*n**	*n*	[15]	[14]
		Part (a)			
9.816	79 157	3.040	3	[79 170][a]	-
		Part (b)			
9.892	79 786	3.092	3	[79 800][a]	-

Assignments, effective quantum numbers and energies E_{Fit} resulting from the fit to Eq. (7) are included. For the error estimated on the present data, see text. At 10.193 eV or 82214 cm^{-1}, the Ly-α transition in free atomic hydrogen is observed (1 eV = 8065.73 cm^{-1} [32]). [a] Data in square brackets: for explanation see text.

4.2.2. The low energy region: analysis using the Rydberg formula [1]

The vibrationless Rydberg series observed for CH_3Cl between 6 and 12 eV are shown in Fig. 2 and their energy positions and assignments are listed in Table 3. In a first step the transitions have been classified according to the nature of the involved Rydberg orbital and by gathering both 3/2-1/2 spin-orbital components. In this table two previous data sets, as reported by Hochmann et al. [14] and Truch et al. [15], have been included for comparison. This table does not include the assignments proposed by these authors. As mentioned earlier, the estimated error on the present measurements is about 4 meV or 30 cm^{-1}. No error estimation being provided by the latter authors, any more critical comparison is made difficult. However, as shown in Table 3, for most of the levels, the correspondence between the three measurements is univocal. It has to be noticed that at 10.193 eV or 82 214 cm^{-1} the Lyman-α transition in the photofragment hydrogen atom is observed. Though within the estimated error limit, it is 44 cm^{-1} below the usually accepted value which is 82258 cm^{-1} [27]. It is an indicator of the accuracy of the photon energy scale.

Obviously, the best agreement is found between the present measurements and the data published by Truch et al. [15]. However, these authors restricted their analysis to the 70 000-90 000 cm^{-1} spectral region missing the structure in the 65 000 cm^{-1} region. For the assignments deduced in the present work, and listed in Table 3, the most accurate adiabatic ionization energies (IE_{ad}) of CH_3Cl as reported by Karlsson et al. [22], i.e. $IE_{ad}(\tilde{X}^2E_{3/2})$ = 11.289 ± 0.003 eV and IE_{ad}-($\tilde{X}^2E_{1/2}$) = 11.316 ± 0.003 eV, have been used.

Concerning the 2e → *n*sa_1 Rydberg series, for both spin-orbit components an average quantum defect δ = 1.07 and 1.06 has been determined. However, the quantum defects vary slightly with the principal quantum number because of the relative evolution of the exchange versus spin-orbit interactions with *n.* This will be dealt with later in this paper. Both values agree very well with each other. The corresponding assignments roughly agree with those proposed by Truch et al. [15] and Hochmann et al. [14]. These authors used 11.223 and 11.303 eV [15] and 11.220 and 11.305 eV [14] for both adiabatic ionization IE_{ad} respectively. Furthermore, it has to be noticed that the former authors do not mention explicitly how the assignments have been ascribed to the lines, e.g. at 88 370 and 88 780 cm^{-1}, to higher lying $9sa_1$ and $l0sa_1$ Rydberg states. Only the latter line fits correctly to a $8sa_1$ whereas the 88 370 cm^{-1} [15] (corresponding to the 88 320 cm^{-1} line in this work) fits at best the $7pa_1$ Rydberg transition. In brackets in Table 3, two lines lying at 11.175 and 11.193 eV respectively could fit in the *n*sa_1 series when the corresponding δ = 1.075 and 1.095 values are considered. However, as it will be shown in the following discussion, these lines could also fit members of the *n*pa_1 series. The same ambiguity exists for the 11.030 eV transition (or 89000 cm^{-1} transition in Ref. [15]) which fits in the $8sa_1(^2E_{1/2})$ and in the $8pa_1(^2E_{3/2})$ series with appropriate quantum defects. On the other hand, the total observed intensity could be the result of the sum of the different contributions.

Apart from the two convergence limits associated with the spin-orbit splitting, a further distinction

appears for the 2e → *n*p Rydberg series depending on the a_1 or e symmetry of the p orbital. These two series differ by a quite different quantum defect. Truch et al. [15] made also a distinction between two *n*p Rydberg transitions, only on the basis of the similarity of the associated vibrational structure (see the discussion in the accompanying paper). However, to both series they ascribed the same quantum defect of $\delta = 0.5$, in disagreement with the present results. Two reasons will lead to discrepancies of the assignments between Truch et al. [15] and this work: (i) the constraint of the constant δ value as used in Truch's work, whatever the nature of the involved Rydberg orbital, and to a less extent (ii) the difference of the IE_{ad} used (more sensitive for higher *n* values).

In the present work, a first series of Rydberg transitions are characterized by an average quantum defect value $\delta = 0.68$ and 0.66. These are observed up to high principal quantum numbers, i.e. $n = 10$ or $n = 13$. These have been ascribed to 2e → *n*pa_1 transitions. They dominate the absorption spectrum and the first term shows the largest absorption cross section. The data in square brackets at 11.175 and 11.193 eV, already mentioned in the above discussion of the 2e → 12*n*sa_1 series, could also fit in the 2e → *n*pa_1 (see (b) series in Table 3), giving rise to quantum defects compatible with a p-character, i.e. $\delta = 0.577$ and 0.483, but significantly different from the values mentioned above.

The second series of Rydberg transitions are characterized by average quantum defects $\delta = 0.438$ and 0.427. These values remain quite constant when the value of the principal quantum number *n* increases. Clearly, these lines pertain to the same series and are ascribed to the 2e → *n*pe transitions. In their rough discussion of the CH_3Cl photoabsorption spectrum, Russell et al. [12] suggested to assign the 74240 cm^{-1} transition (i.e. 74 269 cm^{-1} in this work) to the 2e → 3d transition with a quantum defect $\delta = 0.35$, but do not rule out a 2e → 4p assignment.

The *n*pa_1 orbital is aligned along the C_3 axis and can therefore interact with the a_1 orbitals of the ionic core, leading to some stabilization and thus to a higher term value in contrast to the *n*pe orbitals which are perpendicular to the C_3 axis. It seems therefore more reasonable to assign the largest quantum defect to the *n*pa_1 series [28-30].

Finally, in the photoabsorption 'valley' around 80 000 cm^{-1} (or slightly below 10 eV) two weak narrow peaks and very weak and broader bands are observed. These transitions are much weaker than the s and p transitions. Assuming these signals should correspond to Rydberg transitions, effective principal quantum numbers $n^* = 3.040$ and 3.092 are calculated for both spin-orbit components. With these characteristics, these lines have very likely to be assigned to 2e → 3d transitions. Truch et al. [15] observed these lines at 79 170 cm^{-1} and at 79 800 cm^{-1} and assigned these wavenumbers to 2e → 5sa_1 Rydberg transitions. Hochmann et al. [14] assigned 3e → 3d and 4d doublet transitions to 81666 cm^{-1}, and to 74310 and 82291 cm^{-1} series respectively. In the present work, these transitions were found to fit better a 2e → *n*pe series (see Table 3).

To support this interpretation of the CH_3Cl photoabsorption spectrum, one can lean on the corresponding data for CD_3Cl spectrum reproduced in Fig. 3 between 6 and 12 eV photon energy. The energy positions of the line features are listed in Table 4. As for CH_3Cl, it has to be mentioned that the line at 10.201 eV (82 276 cm^{-1}) is assigned to the Lyman-α line from the D-photofragment atom. This value is slightly lower, but in the error limit of the accepted spectroscopic value of 82 281 cm^{-1} [27].

To make any assignment by using the Rydberg formula, one needs the values of the ionization limits and those of the quantum defects. The latter quantities could be obtained for the different series from the analysis of the CH_3Cl photoabsorption spectrum: they are not supposed to be altered by the isotopic substitution. The former quantity has to be measured. It can first be estimated by applying the Rydberg formula, to any line in the spectrum. For instance the transition at 7.789 eV, corresponding to a 2e → 3 s Rydberg state, has $n^* = 1.963$ so that an ionization limit of $IE_{ad}(\tilde{X}^2E_{3/2}) = 11.320$ eV is derived for CD_3Cl.

To confirm this result, the He(I) photoelectron spectrum of $CD_3Cl^+(\tilde{X}^2E)$ band has been recorded by 1 meV increments over 1024 channels. A mixture of Ar/Kr/Xe is introduced simultaneously for electron energy scale calibration. The lowest ionization energy, i.e. $CD_3Cl+(\tilde{X}^2E_{3/2}) = 11.319 \pm 0.004$ eV has been determined with respect to the three rare gas ions doublets [31]. The resolution of about 25-30 meV is not sufficient to resolve the $^2E_{3/2}$-$^2E_{1/2}$ spin-orbit splitting. However, the very good agreement between photoelectron spectro-scopy and the Rydberg series convergence limit allows us to estimate the ionization energy of the $^2E_{1/2}$ spin-orbit component. Using $n^* = 1.988$, the value of $IE_{ad}(\tilde{X}^2E_{1/2}) = 11.346$ eV is obtained. These two values of the convergence limits will be used throughout for the analysis of the CD_3Cl photoabsorption spectrum.

A long Rydberg series is observed for the 2e → *n*sa_1 transitions, where the principal quantum number $n = 3$-13 is observed for both components of the spin-orbit splitting converging respectively to $\tilde{X}^2E_{3/2}$ [(a) in Table 4] and $\tilde{X}^2E_{1/2}$ [(b) in Table 4]. For both components the quantum defects $\delta = 1.038$ and 0.968 are determined, as averaged over about 10 transitions.

Published in: Chemical Physics (2001), vol. 272, pp. 259-275.
Status: Postprint (Author's version)

Table 4 *Vibrationless Rydberg transitions as observed in CD_3Cl in the present work for both spin-orbit components: parts (a) and (b) converge to the 3/2 and 1/2 components of the ionic ^2E state respectively*

1. $2e \rightarrow n sa_1$

E_{Ryd} (eV)	E_{Ryd} (cm^{-1})	n^*	E_{Fit} (eV)
	Part (a)		
7.789	62815	1.963	7.789
9.786	78 931	2.978	9.775
10.450	84287	3.955	10.457
10.761	86795	4.933	10.769
10.930	88 158	5.906	10.938
11.047	89 102	6.958	11.039
11.100	89 530	7.955	11.105
11.152	89 949	8.999	11.150
11.184	90207	10.002	11.182
11.207	90 393	10.973	11.206
11.225	90 538	11.967	11.224
	Part (b)		
7.903	63 743	1.988	7.905
9.820	79 205	2.986	9.817
10.489	84 601	3.985	10.487
10.809	87 182	5.035	10.797
10.956	88 368	5.909	10.965
11.076	89 336	7.104	11.066
11.136	89 817	8.057	11.132
11.181	90 183	9.092	11.177
11.209	90 406	9.980	11.209
11.235	90 554	11.091	11.233
11.253	90 764	12.121	11.251

2. $2e \rightarrow n pa_1$

E_{Ryd} (eV)	E_{Ryd} (cm^{-1})	n^*	E_{Fit} (eV)
	Part (a)		
8.833	71 245	2.339	8.833
10.110	81 544	3.353	10.103
10.591	85 424	4.320	10.599
10.834	87 384	5.291	10.844
10.980	88 562	6.326	10.982
11.074	89 320	7.437	11.067
11.122	89 707	8.289	11.124
-	-	-	
[11.193][a]	90 280	10.350	11.192
-	-	-	
11.244	90 691	13.338	11.230
11.253	90 764	14.358	11.243
11.263	90 844	15.450	11.253
	Part (b)		
8.909[5]	71 866	2.363	8.908
10.128	81 690	3.342	10.139
10.635	85 779	4.374	10.628
10.879	87 747	5.398	10.872
11.008[5]	88 788	6.349	11.009

2. $2e \rightarrow n pa_1$

E_{Ryd} (eV)	E_{Ryd} (cm^{-1})	n^*	E_{Fit} (eV)
11.097	89 505	7.392	11.094
11.151	89 941	8.353	11.151
[11.193][a]	90 280	9.461	11.190
11.218	90 481	10.310	11.219
-	-	-	

-	-	-	
11.268	90 885	13.380	11.270
11.281	90 990	14.468	11.280
11.290	91 062	15.587	11.288
11.295	91 102	16.333	11.295

3. 2e → *n*pe

E_{Ryd} (eV)	E_{Ryd} (cm^{-1})	*n**	*n*
	Part (a)		
9.222	74 382	2.547	3
[10.239][a]	82 585	3.549	4
10.668	86 045	4.571	5
10.879	87 747	5.561	6
11.008	88 787	6.614	7
11.076	89 336	7.483	8
	Part (b)		
9.301	75 019	2.580	3
10.280	82 916	3.574	4
10.693	86 247	4.568	5
10.905	87 957	5.580	6
-	-	-	7
11.100	89 594	7.577	8
11.161	90 013	8.374	9
[11.193][a]	90 280	9.492	10
11.218	90 522	10.560	11

4. 2e → *n*d

E_{Ryd} (eV)	E_{Ryd} (cm^{-1})	*n**	*n*
	Part (a)		
9.820	79 205	3.012	3
10.470	84 448	4.001	4
10.782	86 965	5.029	5
10.942	88 255	6.000	6
11.043	89 070	7.008	7
11.106	89 578	7.974	8
	Part (b)		
9.895	79 810	3.062	3
10.528	84 916	4.079	4
10.809	87 182	5.064	5
10.980	88 562	6.100	6
11.076	89 336	7.104	7

Assignments, effective quantum numbers and energies E_{Fit} resulting from the fit to Eq. (7) are included. At 10.201 eV or 82279 cm^{-1}, the Ly-α transition in free atomic deuterium is observed (1 eV = 8065.73 cm^{-1} [32]). [a] Data in square brackets: see text.

No comparison can be made with previous measurements. To our best knowledge, the vacuum UV photoabsorption spectrum of CD_3Cl over the 6-12 eV photon energy range has never been reported earlier. The only known UV spec-troscopic work on CD_3Cl has been reported by Felps et al. [10], but this study was limited to the 165-145 nm (61 000-69 000 cm^{-1}) spectral region. In this range two vibrationless Rydberg transitions take place, i.e. at 62 835 and 63 785 cm^{-1} [10] which have to be compared with 62 815 and 63 743 cm^{-1} measured in this work (see Table 4). The small scattering of the δ values, particularly for the Rydberg series converging to $\tilde{X}^2E_{3/2}$, tends to favor the present assignments. Simultaneously, the comparison between the data for the non-deuterated and the deuterated species provides us with stronger support for the proposed assignments in CH_3Cl. In the present case, the isotopic shift on the 0-0 transitions considerably disentangles the spectrum.

As is the case for CH_3Cl, the photoabsorption spectrum of CD_3Cl shows long 2e → *n*pa$_1$ and 2e → *n*pe series converging to both $^2E_{3/2}$ and $^2E_{1/2}$ spin-orbit components. For the *n*pa$_1$ series, principal quantum numbers up to 17 are observed. The 2e → *n*pe is shorter and shows up to *n* = 11. As observed previously for CH_3Cl, averaged quantum defects δ = 0.65 and δ = 0.61 (instead of 0.68 and 0.66 in CH_3Cl) whereas δ = 0.458 and δ = 0.462 (instead of 0.44 and 0.43 for CH_3Cl) are deduced for the *n*pa$_1$ and *n*pe Rydberg transitions respectively.

Published in: Chemical Physics (2001), vol. 272, pp. 259-275.
Status: Postprint (Author's version)

Contrarily to the observations made in the CH_3Cl spectrum, those related to the 2e → *n*d and *n*d' transitions in CD_3Cl give rise to longer and better defined Rydberg series characterized by average quantum defects δ = -0.004 and δ = -0.081. Only one transition was observed in CH_3Cl where δ = -0.040 and δ = -0.092 were determined. The good agreement between these values tends to support the classification suggested for the peaks at 9.815 and 9.889 eV in the spectrum of CH_3Cl (see Table 3). Furthermore, the two lines at 9.820 and 9.895 eV observed in the CD_3Cl spectrum show about the same intensity. Leaning on these arguments, the Rydberg series characterized by these low δ values are assigned to the same 2e → *n*d transitions.

4.2.3. The low energy region: exchange versus spin-orbit interactions

In the low *n* regime, the $(2e)^3(nla_1)$ configuration leads to a ^3E and a ^1E state, which are separated by an interval equal to 2*K* where *K* is the exchange integral (see Fig. 4). When the spin-orbit coupling is switched on, the ^3E state is further split into two E states, one A_1 state and one A_2 state. If the C_{3v} field for these Rydberg states is approximated as nearly cylindrical ($C_{\infty v}$), then the projection of the total electronic angular momentum on the cylinder axis is a constant of motion. One of the E states deriving from the ^3E corresponds to $\Omega = 2$, the other one to $\Omega = 1$, whereas $\Omega = 1$ applies for the ^1E. When *n* increases, the singlet-triplet splitting decreases as $(n^*)^{-3}$ so that the spin-orbit coupling constant *A* becomes comparable with *K*. The spin-orbit operator H^{SO} is able to couple the ^1E (Ω = 1) and ^3E ($\Omega = 1$) substates. Their mixing increases with *n* to reach eventually a 1:1 ratio corresponding to Hund's case (c). In this latter regime, two series with the same quantum defect should converge respectively to CH_3Cl^+ $^2E_{3/2}$ and $^2E_{1/2}$.

Out of the five states which correspond to the $(2e)^3$ (nla_1) configuration, the dipolar transition probability from the ground state $\tilde{X}^1A_1$ of CH_3Cl will be shared between ^1E (Ω = 1) and ^3E (Ω = 1) with an intensity ratio governed by the *K/A* ratio. In a pure Hund's case (c) situation the intensity ratio is equal to 1. In the pure Hund's case (a) the transition to ^3E is forbidden.

Fig. 4. *Coupling scheme corresponding to $(2e)^3(nla_1)$ configuration in both Hund's cases (a) (K >> A) and (c) (K << A) and the intermediate situation. In this figure, A is maintained constant and K decreases from left to right, so that this directly applies to low n states (left) and high n states (right).*

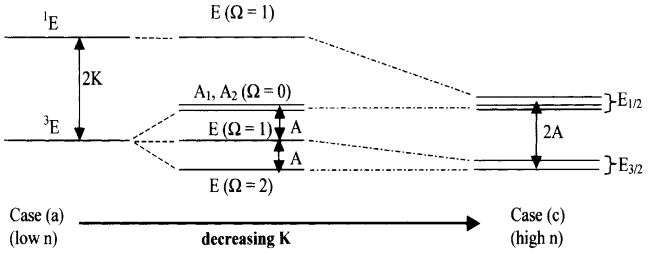

Let us now derive a relationship for the Rydberg state energies valid in the whole coupling range. We will choose Hund's case (a) wave functions as the basis set and then switch on the spin-orbit coupling. In Hund's case (a) the Rydberg states energies are given by Eqs. (2) and (3):

$$E' = E(^3\mathrm{E}) = \bar{E}^{\mathrm{ion}}_{^2\mathrm{E}} - \frac{R}{(n-\delta')^2} \qquad (2)$$

$$E'' = E(^1\mathrm{E}) = \bar{E}^{\mathrm{ion}}_{^2\mathrm{E}} - \frac{R}{(n-\delta'')^2} \qquad (3)$$

where $\bar{E}^{\mathrm{ion}}_{^2\mathrm{E}}$ is the ionization energy which would be observed if the spin-orbit coupling were absent. In practice, it is the average ionization energy as defined by

$$\bar{E}^{\mathrm{ion}}_{^2\mathrm{E}} = \tfrac{1}{2}[E^{\mathrm{ion}}_{^2\mathrm{E}_{3/2}} + E^{\mathrm{ion}}_{^2\mathrm{E}_{1/2}}].$$

As the triplet state is more stable than the singlet, $\delta' > \delta''$.

The total Hamiltonian, including spin-orbit interaction is given by,

$$H = H_0 + H^{\mathrm{SO}} \qquad (4)$$

and the matrix elements are the following:

$$\left.\begin{aligned}\langle {}^3\mathrm{E}_{\Omega=1}|H|{}^3\mathrm{E}_{\Omega=1}\rangle &= \langle {}^3\mathrm{E}_{\Omega=1}|H^0|{}^3\mathrm{E}_{\Omega=1}\rangle = E' \\ \langle {}^1\mathrm{E}_{\Omega=1}|H|{}^1\mathrm{E}_{\Omega=1}\rangle &= \langle {}^1\mathrm{E}_{\Omega=1}|H^0|{}^1\mathrm{E}_{\Omega=1}\rangle = E'' \\ \langle {}^1\mathrm{E}_{\Omega=1}|H|{}^3\mathrm{E}_{\Omega=1}\rangle &= \langle {}^1\mathrm{E}_{\Omega=1}|H^{\mathrm{SO}}|{}^3\mathrm{E}_{\Omega=1}\rangle = A\end{aligned}\right\} \qquad (5)$$
$$\langle {}^1\mathrm{E}_{\Omega=1}|{}^3\mathrm{E}_{\Omega=1}\rangle = 0.$$

The eigenvalues E of the total Hamiltonian are the roots of the following secular equation:

$$\begin{vmatrix} E'-E & A \\ A & E''-E \end{vmatrix} = 0. \qquad (6)$$

They are given by

$$\begin{aligned} E &= \frac{E'+E''}{2} \pm \sqrt{\left(\frac{E'-E''}{2}\right)^2 + A^2} \\ &= \frac{E'+E''}{2} \pm \sqrt{K^2+A^2}. \end{aligned} \qquad (7)$$

It is easy to show that Eq. (7) reduces to Hund's case (a) when $K >> A$ (small *n)* and to Hund's case (c) when $K << A$ (large *n)*. In this case, inserting Eqs. (2) and (3) into Eq. (7) and expanding in powers of n^{-1} leads to two Rydberg series:

$$E^+ = E^{\mathrm{ion}}_{^2\mathrm{E}_{1/2}} - \frac{R}{(n-\overline{\delta})^2} \qquad (8)$$

$$E^- = E^{\mathrm{ion}}_{^2\mathrm{E}_{3/2}} - \frac{R}{(n-\overline{\delta})^2} \qquad (9)$$

with $\overline{\delta} = (\delta' + \delta'')/2$. Two series with the same average quantum defect converge to the two spin-orbit components of the ionic state.

We fitted the energies of the *n*sa$_1$ and *n*pa$_1$ series to Eq. (7) by assuming no n variation of the δ' and δ'' quantum defects. The spin-orbit coupling constant A has been taken as half the ionic $^2\mathrm{E}_{3/2}$-$^2\mathrm{E}_{1/2}$ splitting (see Fig. 4), i.e. 13.5 meV [22]. The fitted energies (labeled as E_{Fit}) are mentioned in Tables 3 and 4. One typical example (*n*sa$_1$ in CD_3Cl) is illustrated in Fig. 5. Table 5 summarizes the results.

Some aspects deserve to be pointed out. (i) The fit of Eq. (7) with constant quantum defects, i.e. with only two free parameters, seems appropriate to account for the experimental data. (ii) We have treated here only the 2e → *n*la$_1$ series. The coupling scheme corresponding to states deriving from 2e → *n*pe is more complicated and has not been dealt with in this paper. (iii) The simple Rydberg formula (Eq. (1)) is only valid in Hund's case (c), i.e. when presently $n \geq 7$. If it is nevertheless applied in the whole n range, then a monotonous variation of the quantum defect with n is expected. This is in fact what is observed in the data of Tables 2 and 3, even though the quantum defects deduced from Eq. (1) are experimentally not very reliable for high n values, because tiny fluctuations result here in huge quantum defects variations. (iv) The values obtained for the exchange parameter K are consistent with the singlet-triplet splitting deduced as early as 1942 by Mulliken for CH_3Cl [33]. (v) One aspect remains unsolved: the intensity ratio corresponding to respectively $^3\mathrm{E}_{\Omega=1}$ and $^1\mathrm{E}_{\Omega=1}$ should be small for n = 3 and should tend to 1 for higher n values. This behavior at low n's is not observed experimentally, neither by us nor by all previous authors [10-15,18]. It must be emphasized that no other assignment seems tractable for the whole set of experimental data presented in the present and in the accompanying paper. In particular, the proposed assignments allow us to account not only for the electronic terms but also for the vibrational structure (paper II of this series). All previous investigators adopted the same assignment for n = 3—one state converging to CH_3Cl^+ $^2\mathrm{E}_{3/2}$, the other one to CH_3Cl^+ $^2\mathrm{E}_{1/2}$— without explicitly mentioning the difficulty associated with the intensity ratio. Some arguments might be invoked here and could be the starting point for further investigations. The 2e → *n*sa$_1$ transition is superimposed on a broad structure which could correspond to a valence-to-valence transition; perturbations affecting the intensities could then be expected. On the other hand, perturbations between the 2e → *n*pa$_1$ and 2e → *n*pe series could also take place. Finally the role of vibronic couplings associated with the Jahn-Teller interaction (see paper II of this series) should also be considered in more detail.

Published in: Chemical Physics (2001), vol. 272, pp. 259-275.
Status: Postprint (Author's version)

Fig. 5. *Comparison between the experimental and the fitted energy values for the $(2e)^3(nsa_1)$ Rydberg series in CD_3Cl. To visually disentangle the data, the n values for the series converging to CD_3Cl^+ ($^2E_{1/2}$) have been slightly shifted along the horizontal axis.*

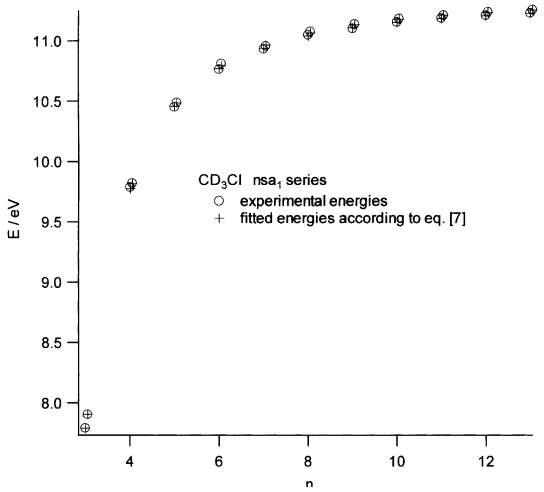

Table 5 *Calculated quantum defects δ' and δ" obtained by fitting Eq. (7) to the data related to the nsa_1 and the npa_1 series in CH_3Cl and CD_3Cl, standard deviation (σ) between the experimental and fitted energies (meV) and values of K exchange coupling element for n = 3 in meV (cm^{-1})*

	CH_3Cl		CD_3Cl	
	$n$sa$_1$	$n$pa$_1$	$n$sa$_1$	$n$pa$_1$
δ'	1.040	0.656	1.040	0.666
δ''	1.009	0.612	1.008	0.633
σ	7	21	6	6
K (n = 3)	55 (441)	45 (365)	56 (455)	35 (279)

5. Conclusions

The vacuum UV photoabsorption spectrum has been reexamined in detail between 6 and 25 eV photon energy. A few weak diffuse absorption bands have been observed in the 12-24 eV photon energy range. These were essentially assigned to 3s Rydberg states, members of series converging to $3a_1^{-1}$, $1e^{-1}$ and higher ionization limits [24]. Very likely a many electron transition is present near 20 eV [24].

In the 6-12 eV photon energy range, many lines spread between 7 and 11.5 eV and are assigned to Rydberg series converging to the spin-orbit split $\tilde{X}^2E_{3/2}$-$^2E_{1/2}$ ground state of CH_3Cl^+. Vibration-less Rydberg transitions have been classified on the basis of their quantum defect.

First, using the simple Rydberg formula, this quantity is reasonably constant for one orbital-type transition. By this way four Rydberg series for each spin-orbit component have been detected: $n$sa$_1$ (δ = 1.069 and 1.064), $n$pa$_1$ (δ = 0.68 and 0.66), $n$pe (δ = 0.438 and 0.427) and finally nd (δ = -0.040 and -0.092). In an earlier work [15] the δ value was assumed to be fixed, e.g. for $n$pa$_1$ and $n$pe series. This led to many differences in the assignments made in this work and in Ref. [15].

To confirm the present interpretation, the photoabsorption spectrum of CD_3Cl has been investigated for the first time. Assignments were made by the same procedure. Also in this molecule the quantum defects remain fairly constant for one orbital-type transition and their values significantly differ for $n$pa$_1$ (δ = 0.651 and 0.610) and for $n$pe (δ = 0.458 and 0.462). The isotopic shift on the vibronic transition allowed us to observe longer nd and nd' series.

In a second step, the magnitude of the exchange interaction, leading to singlet-triplet splitting, and the spin-orbit coupling are considered. The resulting formula [7] for the Rydberg energies accounts for the smooth transition from Hund's case (a) (n = 3, 4) to Hund's case (c) ($n \geq 7$). Good quality fits of the experimental data to the theoretical formula could be obtained with constant quantum defects in the whole observed n range.

This kind of analysis is an essential prerequisite for a detailed interpretation of the threshold photoelectron, constant ion state spectra and ion yield in photoionization mass spectrometry.

Acknowledgements

We are indebted to the University of Liège, the Freie Universität Berlin and the Bundesministerium für Forschung und Technologie for financial support. R.L., B.L. and A.H. gratefully acknowledge the European Community for its support through its TMR programme (Contract EU-TMR-ERBFMGE-CT-970123). H.B. acknowledges the Fonds der Chemischen Industrie for financial support. B.L. thanks the Fonds National de la Recherche Scientifique (Belgium) for a research associate position. This work has also been supported by the Direction de la Recherche Scientifique de la Communauté Française de Belgique through an Action de Recherche Concertée (A.R.C.).

References

[1] M.A.K. Khalil, in: P. Febian, O.N. Singh (Eds.), The Handbook of Environmental Chemistry, Part 4E: Reactive Halogen Compounds in the Atmosphere, Springer, Berlin, 1999, p. 52.

[2] M.J. Kurylo, J.M. Rodriguez, in: D.L. Albritton, P.J. Aucamp, G. Mégie, R. Watson (Eds.), Scientific Assessment of Ozone Depletion, 1998, vol. 1, World Meteorol. Org., Glob. Ozone Res. Monit. Proj., Rep. no. 44, Geneva, 1999.

[3] J. Momigny, R. Locht, Chem. Phys. Lett. 211 (1993) 161.

[4] A. Hoxha, R. Locht, A.J. Lorquet, J.C. Lorquet, B. Leyh, J. Chem. Phys. 111 (1999) 9259.

[5] K.M. Weitzel, F. Güthe, J. Mähnert, R. Locht, H. Baumgärtel, Chem. Phys. 201 (1995) 287.

[6] F. Güthe, R. Locht, B. Leyh, H. Baumgärtel, K.M. Weitzel, J. Phys. Chem. A 103 (1999) 8404.

[7] R. Locht, J. Momigny, in: F. Lahmani (Ed.), Photophysics and Photochemistry above 6 eV, Elsevier, Amsterdam, 1985, p. 171.

[8] W. Zhang, G. Cooper, T. Ibuki, C.E. Brion, Chem. Phys. 137 (1989) 391; W. Zhang, G. Cooper, T. Ibuki, C.E. Brion, Chem. Phys. 151 (1991) 343; W. Zhang, G. Cooper, T. Ibuki, C.E. Brion, Chem. Phys. 153 (1991) 491, and references therein.

[9] J.W. Au, G.R. Barton, C.E. Brion, Chem. Phys. 221 (1997) 151, and references therein.

[10] S. Felps, P. Hochmann, P. Brint, S.P. McGlynn, J. Mol. Spectr. 59 (1976) 355.

[11] W.C. Price, J. Chem. Phys. 4 (1936) 539.

[12] B.R. Russell, L.O. Edwards, J.W. Raymonda, J. Am. Chem. Soc. 95 (1973) 2129.

[13] J.W. Raymonda, L.O. Edwards, B.R. Russell, J. Am. Chem. Soc. 96 (1974) 1708.

[14] P. Hochmann, P.H. Templet, H.T. Wang, S.P. McGlynn, J. Chem. Phys. 62 (1975) 2588.

[15] D.T. Truch, D.R. Salomon, D.A. Armstrong, J. Mol. Spectr. 78 (1979) 31.

[16] C.Y.R. Wu, L.C. Lee, D.L. Judge, J. Chem. Phys. 71 (1979) 5221.

[17] L.C. Lee, M. Suto, Chem. Phys. 114 (1987) 423.

[18] T.N. Olney, G. Cooper, W.F. Chan, G.R. Burton, C.E. Brion, K.H. Tan, Chem. Phys. 205 (1996) 421.

[19] A. Hoxha, R. Locht, B. Leyh, D. Dehareng, K. Hottmann, H.W. Jochims, H. Baumgärtel, Chem. Phys. 260 (2000) 237.

[20] R. Locht, B. Leyh, W. Denzer, G. Hagenow, H. Baumgärtel, Chem. Phys. 155 (1991) 407.

[21] R. Locht, B. Leyh, A. Hoxha, D. Dehareng, H.W. Jochims, H. Baumgärtel, Chem. Phys. 257 (2000) 283.

[22] L. Karlsson, R. Jadrny, L. Mattsson, F.T. Chau, K. Siegbahn, Phys. Scripta 16 (1977) 225.

[23] W. Von Niessen, L. Åsbrink, G. Bieri, J. Electron. Spectrosc. Relat. Phenon. 26 (1982) 173.

[24] R. Locht, B. Leyh, A. Hoxha, D. Dehareng, H.W. Jochims, K. Hottmann, H. Baumgärtel, Chem. Phys. 272 (2001) 293.

[25] R. Locht, B. Leyh, K. Hottmann, H.W. Jochims, H. Baumgärtel, BESSY Jahresber. 1996, p. 162.

[26] J. Berkowitz, Photoabsorption, Photoionization and Photoelectron Spectroscopy, Academic Press, New York, 1979.

[27] C.E. Moore, Atomic Energy Levels, vol. I, Circ. 467, US Dpt. Commerce, N.B.S. Washington, DC, 1949.

[28] J. Schander, B.R. Russell, J. Mol. Spectr. 65 (1977) 379.

[29] L. Singleton, P. Brint, J. Chem. Soc. Faraday Trans. 93 (1997) 11.

[30] R.A. Morgan, M.A. Baldwin, A.J. Orr-Ewing, M.N.R. Ashfold, W.J. Buma, J.B. Milan, C.A. de Lange, J. Chem. Phys. 104 (1996) 6117.

[31] R. Locht, B. Leyh, A. Hoxha, K. Hottmann, H.W. Jochims, H. Baumgärtel, to be published.

[32] E.R. Cohen, B.N. Taylor, J. Phys. Chem. Ref. Data 37 (1973) 663.

[33] R.S. Mulliken, Phys. Rev. 61 (1942) 277.